ENVIRONMENTAL RESEARCH
LETTERS

LETTER • OPEN ACCESS

Global assessment of interannual variability in coastal urban areas and ecosystems

To cite this article: I Odériz *et al* 2024 *Environ. Res. Lett.* **19** 114040

ENVIRONMENTAL RESEARCH
LETTERS

LETTER

Global assessment of interannual variability in coastal urban areas and ecosystems

I Odériz[1,*], I J Losada[1], R Silva[2] and N Mori[3,4]

[1] IHCantabria—Instituto de Hidráulica Ambiental de la Universidad de Cantabria, Santander, Spain
[2] Instituto de Ingeniería, Universidad Nacional Autónoma de México, Mexico City, Mexico
[3] Disaster Prevention Research Institute, Kyoto University, Uji, Japan
[4] Swansea University, Swansea, United Kingdom
[*] Author to whom any correspondence should be addressed.

E-mail: itxaso.oderiz@unican.es

Keywords: coastal hazards, ecosystems, urban areas, ENSO, SAM, AO, long-term risk

Supplementary material for this article is available online

OPEN ACCESS

RECEIVED
22 April 2024

REVISED
13 August 2024

ACCEPTED FOR PUBLICATION
16 September 2024

PUBLISHED
3 October 2024

Abstract

Both seasonal and extreme climate conditions are influenced by long-term natural internal variability. However, in general, long-term hazard variation has not been incorporated into coastal risk assessments. There are coastal regions of high interest, such as urban areas, where a large number of people are exposed to hydrometeorological hazards, and ecosystems, which provide protection, where long-term natural variability should be considered a design factor. In this study, we systematized climate analysis to identify high-interest regions where hazard long-term variability should be considered in risk assessment, disaster reduction, and future climate change adaptation and protection designs. To achieve this goal, we examined the effect of the leading modes of climate variability (Arctic Oscillation, Southern Annular Mode, and El Niño–Southern Oscillation) on the variation in the recurrence of extreme coastal hazard events, including as a first step sea surface temperature, winds, and waves. Neglecting long-term variability could potentially lead to the underperformance of solutions, or even irreversible damage that compromises the conditions of ecosystems for which nature-based solutions are designed.

1. Introduction

In coastal regions, the largest number of people and economic assets that are linked to critical infrastructure, such as ports and airports are concentrated in cities [1]. Windstorms can lead to disruptions in ports [2], causing delays, depreciation of goods, and additional transportation costs [3], with consequential impacts on the global economy [4]. Meanwhile, waves contribute to coastal erosion and flooding [5], to which many coastal areas are exposed.

In addition, mangroves [6], coral reefs [7] and sandy coasts [8] provide coastal protection to human shelters, reducing the economic risk resulting from natural disasters. However, coastal ecosystems naturally experience climate stress. For example, high sea surface temperatures (SSTs) are thermal stressors for coral reefs and are responsible for bleaching and mortality [9]. Mangroves are frequently exposed to extreme winds. Tree mortality and shifts in forest structure are directly dependent on the wind speed. For example, Hurricane Donna in 1960, classified as a category 4 hurricane, caused 25%–100% tree mortality in South Florida [10].

It is well known that interannual variability can lead to changes in seasonal climate conditions [11–15] and extreme events [11, 16, 17] in coastal hazards, including winds, waves and SST. Studies have focused on exploring their impacts on wave conditions in specific planetary regions, such as the Northern Hemisphere [18] and in each ocean basin [12]. Specific modes of climate variability have been the focus of other studies; for example, Odériz *et al* [19] analyzed the El Niño–Southern Oscillation (ENSO), while Marshall *et al* [20] assessed the effect of the Southern Annular Mode (SAM) on ocean waves. The

ENSO also modifies ecosystem functioning [21] by altering SST, serving as an amplifier of heatwaves, as observed during the 1997/1998 El Niño event [22]. Global patterns of long-term variability in near-surface winds have also been studied [12, 23].

The average and extreme conditions of waves (energy and direction), winds (speed and direction), and SST are critical variables for coastal impacts, the operability of certain economic sectors, and the functioning of ecosystems. A description of impacts related to the hazards assessed in this work are summarized in table 1. Understanding long-term exposure to hazards, as documented in historical records, is essential for studying the future trajectories of these systems. Although it is widely accepted that the long-term variability induced by these three modes—ENSO, Arctic Oscillation (AO), and SAM—controls weather patterns with potential repercussions on seasonal coastal risks [24], assessments that can provide knowledge and guidance for long-term risk and coastal protection design have not yet been applied to ecosystems and urban areas in coastal zones, due to a gap in our knowledge of where and which modes can affect coastal hazards.

This study aimed to identify global coastal regions, encompassing ecosystems and urban areas, exposed to long-term hazard variability. The analysis is based on the long-term variability in the seasonal and extreme conditions of coastal hazards (e.g. ocean waves, winds and SST) influenced by the ENSO, AO, and SAM.

2. Materials and methods

In this study, we selected climate variables related to impacts, examining both seasonal averages and extreme conditions in urban areas, mangroves and coral reefs, as indicated in table 1. We then calculated seasonal composite anomalies to evaluate fluctuations in average conditions and to explain teleconnections. Additionally, we analyzed the extreme distribution of seasonal maximum blocks to assess changes in the 20 yr return period (RP20). Extreme analysis was conducted for high-interest areas, with SST analyzed for coral reefs, winds for mangroves, and both winds and waves for coastal urban areas. Finally, we compared the results with the observed events coinciding with the phases of the modes of climate variability (hereinafter climate modes) analyzed in this paper. A brief explanation of the methods is provided below.

2.1. Data

To identify the geographic locations of the exposed regions considered, we selected urban areas located within 0.1° of the shoreline [25]. Coral reefs and mangroves were defined based on the UNEP-WCMC [26] and Bunting *et al* [27] datasets, respectively.

We used climatic parameters from the ERA5 reanalysis dataset [28], covering the period from 1979 to 2018. Seasonal averages were calculated using monthly anomalies of the wind velocity (U_{10}, m s^{-1}), total wave power (P_w, kW h^{-1}), and total swell wave power (P_{sw}, kW h^{-1}). For extreme conditions, maximum values of the SST (MSST, °C), wave power (MP_w, kW h^{-1}), and wind gust speed (MU_{10}, m s^{-1}) derived from hourly time series were employed for each season. The seasons were defined as December, January, and February (DJF), March, April, and May (MAM), July, June, and August (JJA) and September, October, and November (SON).

To identify the positive and negative phases of the different climate modes, the following monthly climate indices from the National Oceanographic and Atmospheric Administration were used: AO (monthly mean AO index), SAM (monthly mean the Antarctic Oscillation (AAO) Index), and ENSO (multivariate ENSO Index version 2, MEI.v2). We focused on the impacts of the AO in the Northern Hemisphere and the SAM in the Southern Hemisphere because the resulting interhemispheric teleconnection may imply complex mechanisms not well demonstrated in the literature.

2.2. Long-term variability under average conditions

In contrast to the SST, winds and waves have critical directional components in terms of the induced coastal impacts. Under seasonal average conditions, the directional component was incorporated by calculating composite anomalies applied to the global wind system and the wave climate conditions proposed by Odériz *et al* [29] (figure S1b). Based on the wind direction and speed, Odériz *et al* [29] classified wind climate into easterlies, westerlies, and southerlies, obtaining an equivalent classification for waves (based on wave power and direction). For each planetary wind system and wave climate, monthly anomalies of the wind velocity (U_{10}), total wave power (P_w) were calculated by subtracting monthly data from the mean of the corresponding month for the full time series (1979–2018). Composite anomalies were calculated as the anomaly mean of the wave or wind climate for the months corresponding to the seasonal timeframe of phase occurrence. Statistical significance was determined using a two-tailed Student's t test at the 95% confidence level, following the methods described by Odériz *et al* [29].

The SST, a scalar variable, was calculated similarly but without including climate classification. For simplicity, this work focused on the positive (+) phases of the AO during DJF, the SAM in JJA, as these seasons have a high impact. The ENSO was considered for all seasons, as it shows a more complex hazard influence that varies from season to season [19].

Table 1. Coastal hazards and related impacts in exposed systems analyzed in this study. References can be found in supplementary information table S1.

		Average hazard conditions and related impacts		Extreme hazard conditions and related impacts	
Exposed system	Coastal hazard	Operativity and functioning of the systems	Reference	Related impacts	References
Urban areas	Wave flux energy and direction	Wave energy production	(Reguero *et al* 2015, 2019)	Coastal flooding	(Andrade *et al* 2013, Melet *et al* 2018, 2020, Toimil *et al* 2020, Wandres *et al* 2020)
		Wave energy production	(Medina Rodríguez *et al* 2023)		
		Port operability	(Diaz-Hernandez *et al* 2021, Romano-Moreno *et al* 2022, 2023)	Port disruptions causing delays, depreciation of goods, and additional transportation costs	(Achurra-Gonzalez *et al* 2019, Camus *et al* 2019, Izaguirre *et al* 2021, Rose and Wei 2013)
		Shoreline shape and position	(Alvarez-Cuesta *et al*, 2021, Barnard *et al*, 2015, Vos *et al* 2023)	Coastal erosion	(Leaman *et al* 2021, Toimil *et al* 2020)
	Wind speed and direction	Port operability	(Zhou *et al* 2020)	Maritime disruptions	(Adam *et al* 2016)
				Damage to energy infrastructure	(Gliksman *et al* 2023)
				1) windthrow and electricity cuts 2) long-lasting power failures affect the energy production, the structural integrity and operational safety of wind turbines	
				Damage to buildings	(Blackmore and Tsokri 2004, Changnon 2009, 2011, Gliksman *et al* 2023)
		Renewable wind energy production	(Carta and Mentado 2007, Nelson 2009)	Damage to transport infrastructure: 1) Local problems with road and rail traffic. 2) Delays and cancellations in air, rail, road traffic and disturbances of ferry traffic 3) Cancellation of rail and road traffic 4) Damage to traffic control devices 5) Structures, airports can be closed, and ferries stay in harbour	(Gliksman *et al* 2023)
				Insurance losses	(Koks and Haer 2020)
Mangroves	Wind speed and direction	Canopy environment	(de Lima and Galvani 2013, Nelson 2009)	Tree mortality	(Craighead and Gilbert 1962, Krauss and Osland 2020, Primavera *et al* 2016)
		Dispersal pollination	(Van Der Stocken *et al* 2013, Van der Stocken and Menemenlis 2017)	Shifts in forest structure	(Kauffman & Cole, 2010; Peereman *et al*., 2022)
Coral reefs	Sea surface temperature	Coral reef environment	(Barber *et al*., 2001; Wernberg *et al*., 2016)	Coral bleaching	(Eakin *et al* 2010, Liu *et al* 2003, Mumby 1999, Stone *et al* 1999)
				Coral mortality	(Eakin *et al* 2010, Elvan Ampou *et al*., 2017; Glynn & D'croz, 1990, Leggat *et al* 2019)

2.3. Seasonal extreme conditions

Extreme analysis was conducted using a nonstationary GEV cumulative distribution function [30], considering changes in block maxima within the analyzed period (1979–2018). This approach has been widely employed for extreme analysis in marine climate studies [11, 17, 31]. The location, shape, and scale of the GEV distribution are time dependent, and climate indices were used as covariates. Initially, coefficients and constants were derived from linear regression of the climate index and GEV parameters, assuming a nonstationary GEV function without covariates. Subsequently, for each season, we calculated the climate index time series, and we detrended and normalized the series, which was then integrated as a covariate of the GEV function.

The Kolmogorov−Smirnov test at the 95% confidence level was applied to verify that the data followed a GEV distribution. For significant results, the 20 yr return period (RP20) was obtained for 1979–2018. The selected return period was chosen as a safety level defined by standards, ensuring confidence in the projections derived from the time series length of each phase. The percentage change in RP20 attributable to the climate modes was calculated as the ratio of the long-term average to the positive phase average. The RP20 of the positive phase is calculated as the average of the RP of the months when the index indicates a positive phase (over 0.5 for MEIv2 and over $\sigma + \mu$ for the AO and AAO indices). Using different threshold for climate indices will analyse the effects of varying intensities of climate modes in extreme events. For example, how weak moderate and strong El Niño modify the intensity of RP20 and their spatial patterns. We considered RP20 values lower than the long-term average return period within the safety levels for urban areas and within the range of tolerable maximum conditions for ecosystems.

3. Long-term hazard variability under average conditions

The long-term SST variability patterns induced by ENSO+ events are well known: warming in the eastern Pacific and cooling in the western Pacific [32]. The findings showed that the Indian Ocean also warms during ENSO+ events, as do some regions of the South Atlantic (figures S2(e) and (f)). Generally, the SST patterns for SAM+ and AO+ were spatially more heterogeneous and less well defined (figures S2(g) and (h)). At mid-latitudes, a temperature increase was observed during AO+ in northeastern regions of the Pacific and Atlantic Oceans.

The results for winds and waves are shown in figure 1. The regions most impacted by each climate mode, with a related increase (decrease) in the swell wave power or wind velocity, are highlighted in red (blue). The arrows indicate the directions of winds and waves in the detected anomalies.

In DJF, during ENSO+ events, extratropical winds intensified in the mid-latitude regions of the Northcentral Pacific ($\sim$+0.5 m s^{-1}), induced by an intensification of the Aleutian Low [33] (figure S2(a)). A decrease in the wind speed was found in the northwest and southeast Pacific (approximately −0.4 m s^{-1}). During this season, westerly swells strengthened in the extratropical regions of the Northeast Pacific ($\sim$+15 kW m^{-1}), in the Southern Ocean, southern Atlantic and Indian Oceans (figure 1(f)). The AO+ phase induced opposing sea level pressure responses at high and mid-northern latitudes (figure S1(c)). During this season, it caused higher wind speeds and wave powers at high latitudes in the Atlantic Ocean ($\sim$+1 m s^{-1}, $\sim$ +23 kW m^{-1}) (figures 1(b) and (e)).

In JJA, SAM+ intensified extratropical winds and waves at high latitudes in the Southern Hemisphere, and conversely, they were weakened at mid-latitudes. Southerly waves are swell-dominated [29], and energetic southerly swells in the Eastern Pacific (figure 1(k)) intensified in JJA due to increased extratropical wave power (+9 kW m^{-1}). However, ENSO+ generated the opposite effect on westerly and southerly swells ($\sim$−4 kW m^{-1}), reducing their energy in the southeastern Pacific. Annular modes and ENSO induce opposite effects on extratropical and southerly swells, which affect the east coast of the Pacific. For these swells, the SAM+ phase (JJA) serves as an amplifying factor. In the Indian Ocean and Pacific Ocean, SAM+ intensified southern tropical winds ($\sim$+0.75 m s^{-1}). However, in the tropical Atlantic, ENSO+ intensified winds up to $\sim$ +2 m s^{-1}, triggering an increase in swells in the Caribbean Sea ($\sim$ +2 kW m^{-1}). ENSO+ intensified monsoon winds ($\sim$ +0.5 m s^{-1}) in the Bay of Bengal. In contrast, in the Arabian Sea, a decrease ($\sim$−0.3 m s^{-1}) in the wind velocity and swell energy ($\sim$ −0.3 m s^{-1}; $\sim$−3 kW m^{-1}) was recorded (figures S3(i)–(l)).

During ENSO+ in MAM (figures S5(g)–(l), (r)), extratropical winds decreased near the Strait of Magellan ($\sim$−0.5 m s^{-1}), while on the Pacific coast of Mexico, they increased. During this season, swells propagating from the west intensified in the northeast Pacific ($\sim$+8 kw m^{-1}) and decreased in South America ($\sim$ −8 kw m^{-1}). In SON, the southern trade winds decreased ($\sim$ −0.75 m s^{-1}), which also affected the southern tropical belt.

4. Long-term hazard variability in extreme events

The results, expressed as changes in the intensity of RP20 events, exhibited patterns similar to those under the average conditions, with some exceptions.

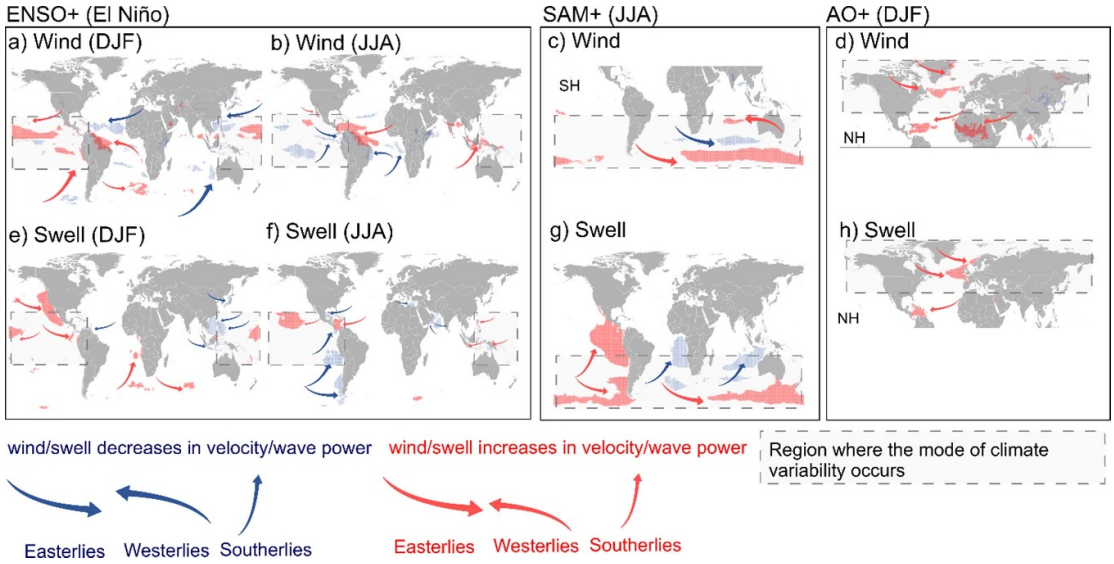

Figure 1. Long-term spatial hazards patterns of wind (a)–(d) and swell (e)–(h) during the positive phases of ENSO+ (DJF and JJA), SAM+ (JJA), and AO+ (DJF).

4.1. SST

The habitat of coral reefs is restricted by the thermal range: between 25 °C and 29 °C [34], while temperatures below 18 °C or over 40 °C cannot be tolerated [35]. In JJA, the RP20 over the entire analysis period showed an increase in the SST from north to south (figure 2(d)), contrasting with the results for DJF (figure 2(a)). This pattern is similar to the seasonal variability in warm waters. The highest RP20 values were found north of Australia in DJF (31 °C) and in the Persian Gulf in JJA (36 °C). Moreover, in the Indian Ocean, the RP20 values were greater in MAM, as shown in figure 2, where Panels a and b show the long-term average RP20 for each season. The black regions denote the locations of coral habitats where significant GEV fitting was not observed.

In DJF, El Niño warmed Caribbean waters by up to 0.4% and the southwest Pacific and west Indian Oceans (Somalia, Kenya, and Tanzania), which is consistent with the seasonal anomalies observed under average conditions. The AO+ increased the RP20 of the SST in the North Mexican Gulf (0.3%) and the Red Sea (0.7%), conforming with the anomalies found under seasonal average conditions (figure S2(g)).

The ENSO warms tropical east Pacific waters, with an increase found here in all seasons, with the greatest increase in JJA, when the RT20 increased by up to 1%. SAM+ showed a notable increase in the warm pool region and northeast of Australia, with the RP20 in the Indo-Pacific, averaging 0.3%, reaching 0.7% in the northern region of the Great Barrier Reef, Australia.

The extreme SST is most affected by ENSO+ in MAM, and the greatest anomalies were found during this period, impacting the Isthmus of Panama, the Red Sea, the Arabian Sea, and Southeast Asia by up to 1.2%. In contrast, in SON, the seasonal variability was less influenced by ENSO+. This finding aligns with the variations obtained under average conditions, where the SST anomalies in MAM extend over large oceanic areas, particularly in the Indian Ocean and Atlantic. In contrast, the anomalies were reduced in SON, especially in these regions.

4.2. Extreme winds

We identified high-interest regions exposed to extreme winds affected by climate modes. Since wind power is proportional to the cube of the wind speed, even minor shifts in speed can result in significant implications for risks. Seasonally, higher RP20 values were found at mid-latitudes due to extratropical winds, while subtropical and tropical regions exhibited lower wind speeds. There were regions with RP20 values of over 40 m s^{-1}: northern Europe in DJF, affected by extratropical cyclones; eastern Asia in JJA and SON; and the eastern USA and Caribbean countries in SON, affected by tropical cyclones (figures 3(a), (d), S6(a), (b)).

In DJF, anomalies in wind patterns induced by AO+ were observed in the West North Pacific, North Europe, and tropical regions, generally without any relevant changes affecting coastal cities, although there were exceptions.

In JJA, ENSO+ impacted many cities, particularly in the northwest Atlantic and northwest Pacific. RP20 values greater than those listed above were found in 3 cities, namely, Coatzacoalcos (Mexico), Kill Devil Hills (USA), and Nassau (Bahamas), with values of up to 7%. SAM+ induced less variation in the RP20 in the Southern Hemisphere for coastal cities, with the maximum value reaching 2.85% for Hobart (Australia).

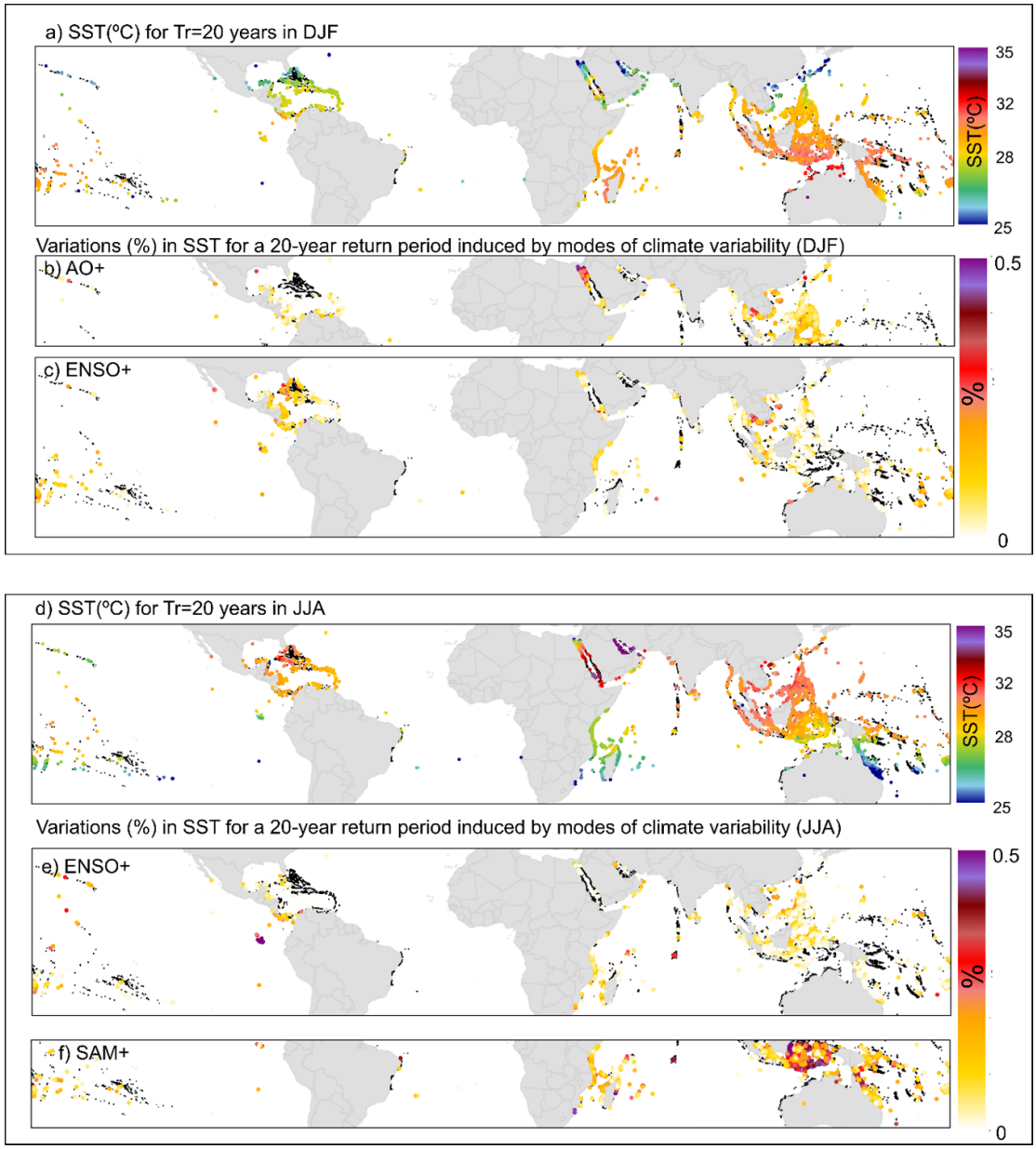

Figure 2. Thermal stress for coral reefs. The 20 yr return period of extreme SST in (a) DJF and variations induced by (b) AO+ and (c) ENSO+. Similarly, for JJA in (d)–(f).

The ENSO+ in MAM exhibited the highest fluctuations for the climate modes analyzed. San Sebastián (Chile) experienced the greatest increase, 25.6%, with no significant variations under average conditions. Other cities in Japan exhibited increases of up to 6%–7% from April to December, marking the start of a typhoon season more intense than normal. In contrast, SON exhibited less spatial extension impacted by ENSO+, with the highest variation in RT20 in Qinzhou (China), at 4.17%.

Mangroves are greatly affected by tropical cyclones, with large regions exposed to high winds, including the northwest of Australia in DJF, the USA (Florida), and China in JJA. In the Southern Hemisphere, SAM+ (JJA) led to a greater increase in extreme winds in mangrove areas than in cities. In DJF, ENSO+ intensified extreme winds over Fiji and northwest of Australia (7.1%). During this season, AO+ affected New Orleans (3.98%), the eastern coast of India (up to 6.15%) and some regions in southern East Asia.

ENSO+ in MAM was again the mode with most influence, with notable anomalies in northern Australia (19.8%), the east coast of Madagascar (10%), and the central Pacific coast of Mexico (8.5%). SON is the season in which fewer impacts of ENSO+ were registered globally, although there were higher values in certain mangrove areas.

4.3. Ocean waves

There were significant variations in the geographical distribution of wave energy during the different

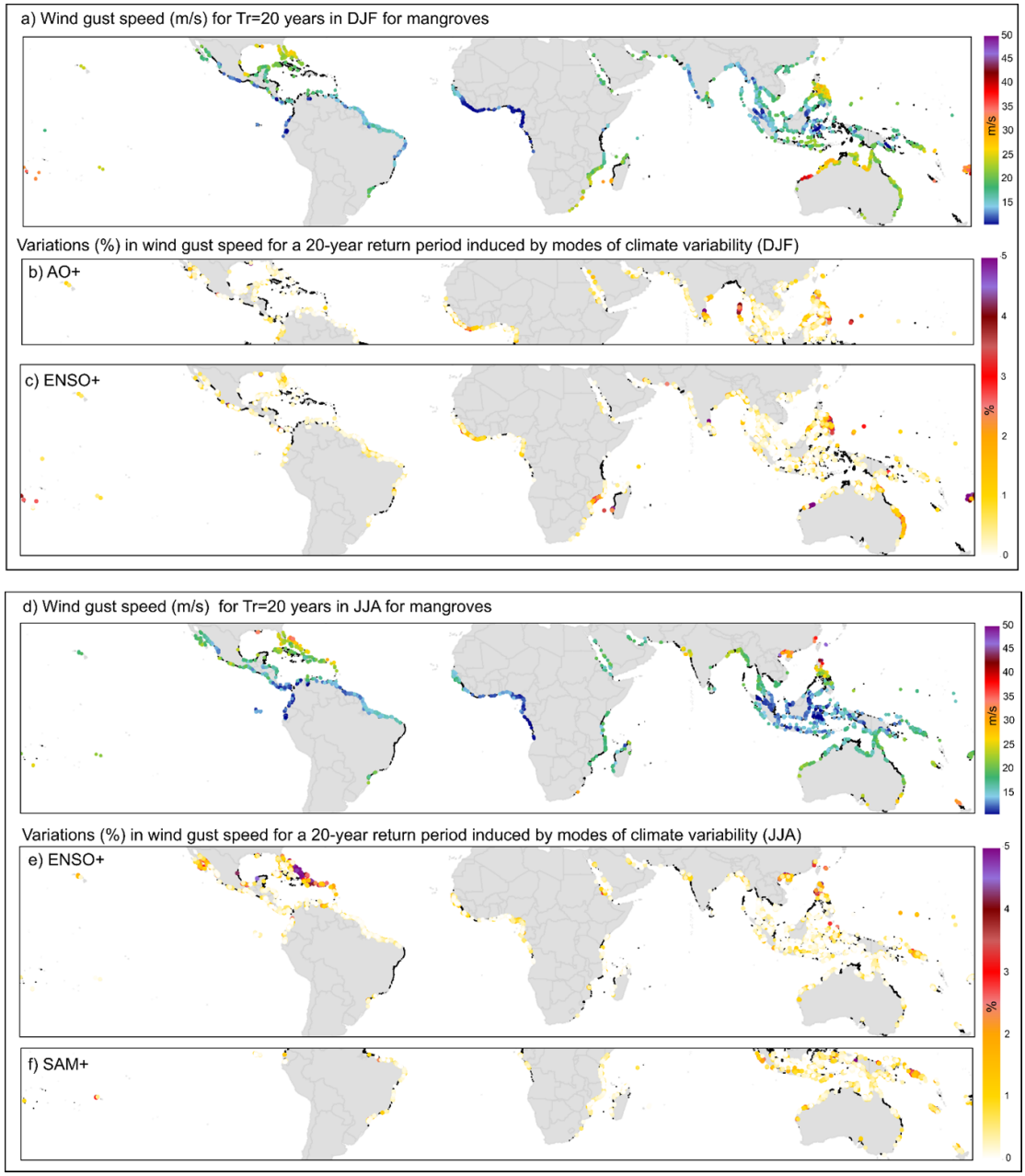

Figure 3. Extreme winds for mangroves. The 20 yr return period of extreme wind gusts speed in (a) DJF and variations induced by (b) AO+ and (c) ENSO+. Similarly, for JJA in (d)–(f).

seasons for the three climate modes, as figure 4 shows. In contrast to winds, the RP20 of waves yielded less clear latitudinal patterns, due to the directional nature of wave propagation. In DJF, the regions with greater return periods include the coasts of Japan, Europe and the USA. South Africa, Madagascar, Australia, and New Zealand also experienced heightened intensity during this season. In JJA, wave energy increased along the coasts of southern America, the west coast of India, and the Gulf of Mexico and Caribbean, primarily influenced by tropical cyclones.

In MAM, under the influence of the ENSO, Torres in southern Brazil experienced a 44.14% increase, while Mahajanga (Madagascar) experienced a 22% increase under RP20. In JJA, ENSO+ affected the west coast of Mexico, Japan, and the northeast Atlantic. Locations such as Þykkvibæ (Iceland) exhibited a substantial increase (105.22%), Kushiro in Japan experienced a 59.55% increase, and Coronel in Chile recorded a 49.34% increase.

The SAM+ phase in JJA induced an increase in the intensity of RP20 in various regions, including Scottburgh in South Africa (164.6%), Old Bar in Australia (49.18%), and Iquique, Dichato and Arica in Chile (up to 66.34%). Cities on the west coast of Mexico (Acapulco) and Indonesia (Bengkulu) were also affected by the intensification of swells originating from the Southern Hemisphere, as suggested by the anomalies found under average conditions.

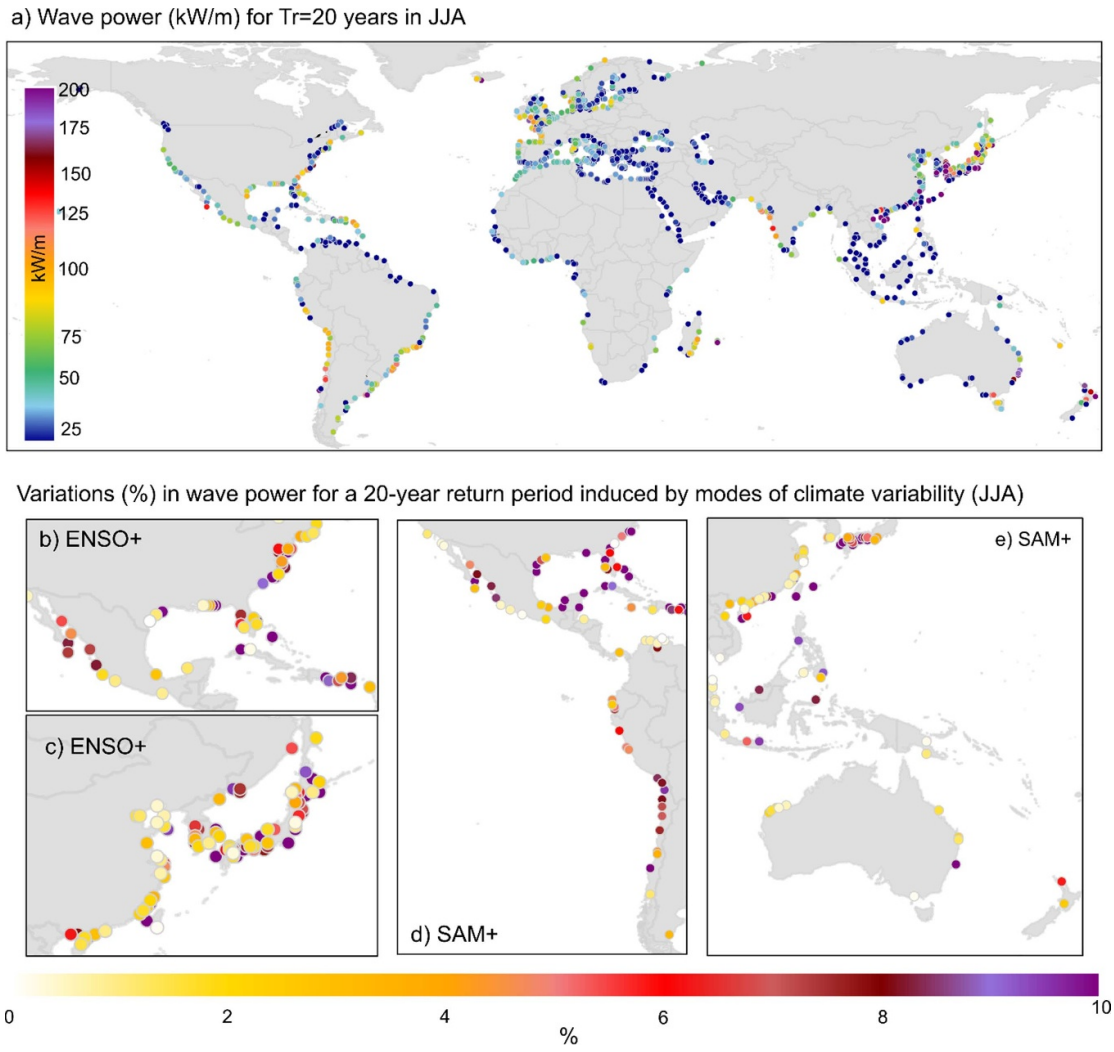

Figure 4. Extreme waves for coastal urban areas. The 20 yr return period of extreme wave power in (a) JJA and variations induced by (c) and (b) ENSO+ and (d) and (e) SAM + .

Interestingly, there was a greater increase in extreme waves on the coasts of Indonesia and Mexico than that in seasonal average conditions.

In DJF, similar to the AO, ENSO+ contributed to increased wave power in cities such as Castletown (UK) and Les Cousteaux (France). Overall, in Europe, the variability in the wave climate during the positive ENSO and AO phases influenced extreme wave conditions in a similar way. The intensification observed in the Caribbean during the SAM was not identified, with swells propagating from the south under average conditions.

5. Discussion

In this section, we explore how the literature on teleconnection mechanisms can explain and support our results. In addition, the potential implementation of the findings in practical applications is described.

5.1. Results consistent with established teleconnection mechanisms and observed extreme events

Identifying the atmospheric and oceanographic mechanisms behind teleconnections is beyond the scope of this study. However, understanding these mechanisms is crucial for determining the role of these modes in the observed variations. Figure 5 shows the regions where the long-term variability affects extreme events. We compare these findings with observations found in the literature.

In thermal stress analysis, the regions where climate modes impact extreme temperatures (figure 5(c)) are Central America, the Arabian Peninsula, the Indo-Pacific region, Mozambique, and Madagascar. The Gulf of Suez, where the AO signal has been detected in historical records [36], is the region most affected by the AO+ phase in DJF. Under the influence of ENSO+, the results showed an increase in the eastern Caribbean Sea, the

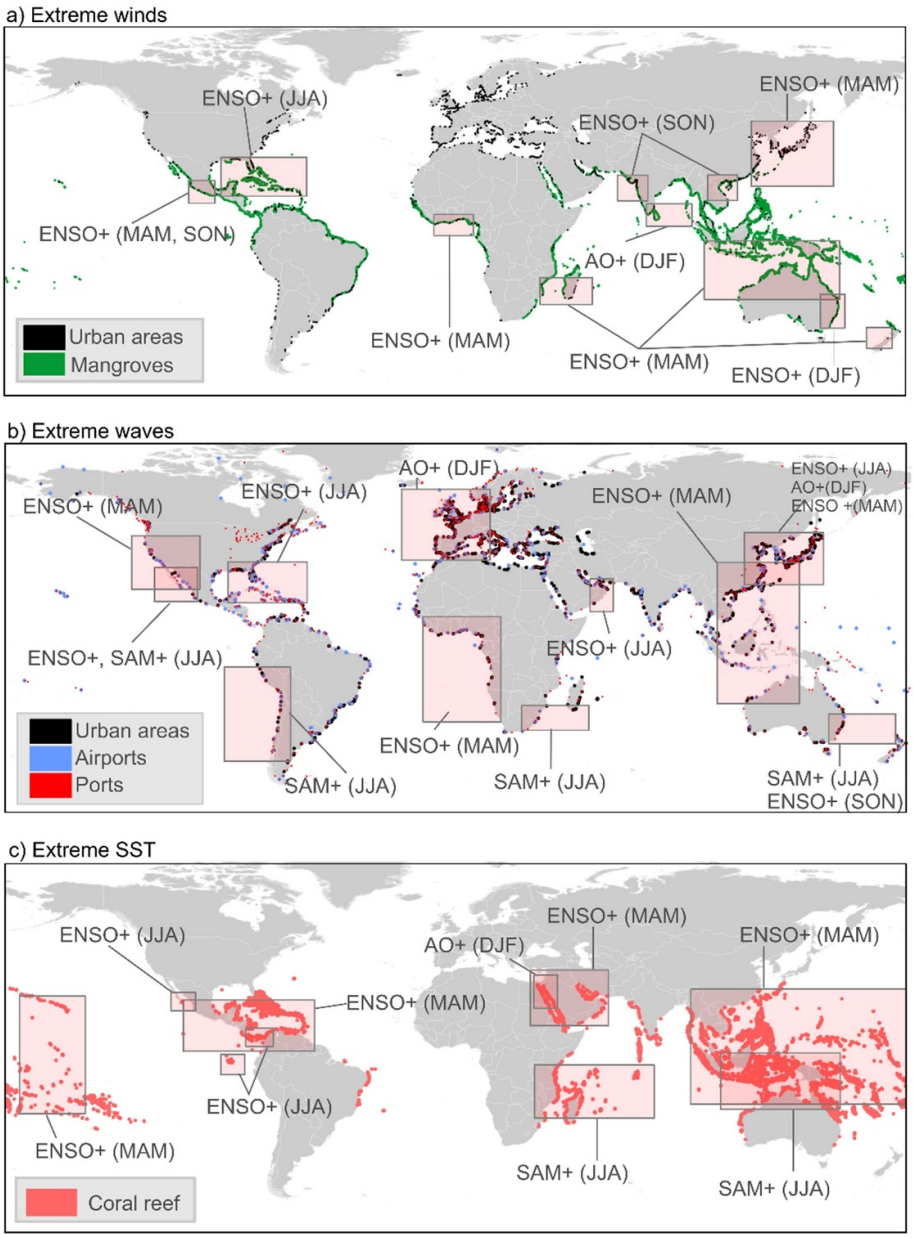

Figure 5. Exposure regions where the modes of climate variability have influenced the 20-year return period for coastal hazards: (a) winds in mangroves and urban areas, (b) waves in urban areas, and (c) SST in coral reefs.

central Indian Ocean, and the eastern Pacific Ocean, where the impacts of the ENSO on coral reefs have been documented [34], such as in the Lakshadweep Archipelago of the Indian Ocean [37]. Our results showed that the Galapagos coral reef is the region most affected during ENSO+ events in JJA. In this region, records exceeded +3 °C during El Niño events from 1982–1983 and 1997–1998 [38]. The variability induced by SAM+ in the coral reefs of the Indo-Pacific was noteworthy in our extreme analysis. Studies have related higher surface temperatures in the southwestern Pacific to heighten positive phases of the SAM [39].

It has been widely demonstrated that tropical and extratropical cyclones are influenced by climate modes. In the North Atlantic, our results showed that winds were intensified during El Niño at the beginning of the hurricane season (JJA), but decreased towards the end of the season (SON). El Niño enhances the frequency and intensity of tropical cyclones in the Pacific [40–42], and our results further underscored the role of ENSO+ in augmenting tropical cyclone activity. In particular, in MAM, typhoon activity increased with smaller increases in JJA and SON. In SON, an increase in the intensity of RP20 along the Mexican Pacific coast was detected. In DJF, the eastern Australian coast was impacted by a more active tropical cyclone season. During ENSO+ events, our results did not show an increase in extreme winds for the northwestern coast of the

USA. In this area, several authors [43, 44] have reported that the frequency of extreme winds decreases during the boreal winter months under El Niño.

Additionally, our results revealed that there are significant correlations between the AO+ phase and extreme wind variations in Europe. However, we observed similar regional patterns for the ENSO and AO. The impacts of the AO in Europe described in this work are consistent with current state-of-the-art findings. In the case of the ENSO, the intensity of RP20 increased with extratropical wind activity, which agrees with previous studies [45]. Conversely, other studies have suggested that ENSO patterns resemble NAO patterns in the European climate [46]. This long-term behavior leads us to hypothesize that the NAO (a similar pattern to that of the AO but restricted to the Atlantic Ocean [15] and not analyzed here) may become a critical mode for this region in the future, where projected changes and internal atmospheric variability cannot be confidently separated [47–49]. Further investigation for this region is needed to better understand the interaction between the ENSO and AO. With our analysis, we could determine that the ENSO and AO interact, but we could not clarify whether our results suggest temporal synchronicity for both climate modes, leading to similar outcomes, or whether there is a teleconnection mechanism that produces these similarities. Consistent with earlier works [13, 19], ENSO+ modifies extratropical waves in the Pacific region. The results shown here demonstrate that ENSO+ is linked to intensification of the northern extratropical wave climate in DJF and MAM and to a decrease in swells coming from the Southern Hemisphere in MAM. Therefore, swells originating from the south are enhanced by the SAM, which explains the energetic swells affecting the Pacific coast of America (from Peru to California) over the last decade [50]. Under average conditions, the ENSO and annular modes induce opposite responses in terms of swell energy off the east coast of the Pacific. The AO+ phase triggers a decrease in the swell energy originating from the west, while ENSO+ strengthens it. In Europe, wave power responds similarly to the ENSO and AO, showing both mode connections, similar to what was determined for extreme winds.

In addition, natural variability is affected by anthropogenic drivers [47, 51]. Many studies suggest that it is likely that the ENSO will intensify [52, 53], as will the positive phase of the annular modes [54, 55]. These changes in natural variability over the next century can have repercussions on future coastal hazards [56], as well as on the spatial regions defined in this work.

5.2. Potential practical implication

In this study, we highlight the fact that seasonal changes in extreme events of the main climate variables related to coastal impacts (SST, winds, and waves) result from weather patterns and interannual variations. These changes have been associated with urban areas and regions where mangroves and coral reefs are located, both of which are valuable, due to the several services they provide. Our study identified regions, shown in figure 5, where long-term variability affects the RP20. This might have implications for seasonal forecasting and risk assessment across these timescales. While it is beyond the scope of this study to demonstrate the consequences of climate modes on coastal risk and adaptation, the information provided on regions at a global scale might be useful for developing in-depth analysis of climate variability for long-term risk reduction, designing nature-based solutions (NbS), or planning the adaptation of urbanized coastal areas. The purpose of this section is to discuss how this study can build a bridge between long-term hazard variability and its implications for risk, adaptation, and NbS designs.

The need for seasonal forecasts has been emphasized by the IPCC [57]. Long-term variability modulates seasonal extreme conditions, and for some regions, the integration of climate modes might be required to guarantee accurate seasonal forecasting. Our results illustrated the changes in intensity of the 20 yr return period (a familiar parameter for risk experts) in response to interannual variations. Future analyses should address how hazard variability and its effects on coastal risk assessment could potentially lead to underestimating the real risk in urban areas.

NbS are promising alternatives for climate change adaptation and disaster risk reduction. However, the long-term response of ecosystems to global change remains highly uncertain, and the effectiveness of NbS may be compromised due to an incomplete understanding of the long-term hazard variability. The biophysical characteristics of ecosystems respond to both average and extreme climate conditions. For instance, the seasonal average of winds plays a crucial role in dispersal pollination [58, 59], while tropical cyclones can modify mangrove forest structures [60, 61]. In this study, we examined the long-term variation in both seasonal average conditions and extreme conditions, recognizing that the resilience of ecosystems, and thus their provided services, may respond in different ways under different climate conditions [62]. This long-term climate variability is a critical element to be incorporated in the design, construction and maintenance of NbS since, in contrast to rigid infrastructure, the biophysical features of NbS (e.g. forest structure, cover, or biomass) can vary with time, affecting their performance in coastal protection. For example, the biophysical features of NbS, which can be modified by long-term climate variability, are crucial for quantifying the coastal protection services provided during their lifetime [63].

6. Conclusions and future work

This study analyzed the exposure of coastal urban areas and ecosystems to long-term hazard variability. In particular, we characterized variability of coastal hazards and identified regions where the seasonal average and extreme conditions of the SST, extreme winds, and waves are modified under the influence of the main polar (AO and SAM) and tropical (ENSO) climate modes. These results show exposed systems (urban areas, mangroves and coral reefs) worldwide.

In general, ENSO increases the intensity of events with a 20 yr return period probability for winds, waves, and SST. Meanwhile, the AO during DJF increases extreme waves intensity related with a RT20 in Europe, and the SAM during JJA increases intensity in Australia, South America, and South Africa. Extreme SSTs with a 20 yr return period increase in intensity due to ENSO during MAM and JJA, SAM in the coral reefs located in the Indo-Asian Ocean, and AO in the Red Sea.

The findings are presented in a manner that is easily interpretable and implementable for stakeholders, and provide information for determining whether these variations should be incorporated into site-specific studies, and this study serves as a reference for future climate consequences.

In future research, efforts should be developed towards analysing climate modes and risk, as neglecting this factor might lead to inappropriate risk reduction planning, protection design, and adaptation measures for some regions. We emphasize the importance of further research on incorporating long-term hazard variation into the design of NbS, since ecosystem services change with climate stress. This can potentially affect the reliability assessment and the design of NbS to ensure the maintenance the required standards for protection during the project's lifetime. This methodology can be applied to other exposed systems, such as critical infrastructure, and to other ecosystems. It can also be extended to include additional hazards, such as precipitation and storm surge. More importantly, these models should be integrated into long-term risk reduction assessments that consider multihazard and multisector scenarios, where cities and ecosystems coexist. Such integration would allow analysis of the consequences for several systems, considering the co-occurrence of hazards, which is essential for a more realistic characterization of our complex world.

Data availability statement

Authors acknowledge the following institutions for providing the data in open access that have made this study possible. These are: the Copenicus Climate Services for the climate variables (https://cds.climate.copernicus.eu/cdsapp#!/dataset/reanalysis-era5-single-levels?tab=overview). The National Oceanographic and Atmosphere Administration for the climate indices (https://psl.noaa.gov/data/climateindices/list/). Mangroves and coral distributions are downloaded from the United Nations Environment Programme (https://data.unep-wcmc.org/). Urban areas are downloaded from the Natural Earth. Free vector and raster map data @ naturalearthdata.com. (www.naturalearthdata.com/downloads/10m-cultural-vectors/).

The data that support the findings of this study are openly available at the following URL/DOI: https://doi.org/10.5281/zenodo.11004723 [64].

Acknowledgments

I O is grateful for financial support through the Juan de La Cierva Program FJC2021-047909-I, funded by MCIN/AEI/10.13039/501100011033 and the European Union NextGenerationEU/PRTR. This study is part of the ThinkInAzul program, supported by Ministerio de Ciencia e Innovación with funding from the European Union NextGeneration EU (PRTR-C17.I1) and the Comunidad de Cantabria. Additionally, it is part of the FENIX Project, funded by the Comunidad de Cantabria.

ORCID iD

I Odériz https://orcid.org/0000-0002-6338-1141

References

[1] Cities, Settlements and Key Infrastructure 2023 *Climate Change 2022—Impacts, Adaptation and Vulnerability* (Cambridge University Press) pp 907–1040
[2] Camus P, Tomás A, Díaz-Hernández G, Rodríguez B, Izaguirre C and Losada I J 2019 Probabilistic assessment of port operation downtimes under climate change *Coast. Eng.* **147** 12–24
[3] Achurra-Gonzalez P E, Angeloudis P, Goldbeck N, Graham D J, Zavitsas K and Stettler M E J 2019 Evaluation of port disruption impacts in the global liner shipping network *J. Ship. Trade* **4** 3
[4] Rose A and Wei D 2013 Estimating the economic consequences of a port shutdown: the special role of resilience *Econ. Syst. Res.* **25** 212–32
[5] Toimil A, Camus P, Losada I J, Le Cozannet G, Nicholls R J and Idier D 2020 Climate change-driven coastal erosion modelling in temperate sandy beaches: methods and uncertainty treatment *Earth Sci. Rev.* **202** 103110
[6] Menéndez P, Losada I J, Torres-Ortega S, Narayan S and Beck M W 2020 The global flood protection benefits of mangroves *Sci. Rep.* **10** 1–11
[7] Beck M W, Losada I J, Menéndez P, Reguero B G, Díaz-Simal P and Fernández F 2018 The global flood protection savings provided by coral reefs *Nat. Commun.* **9** 2186
[8] Toimil A, Losada I J, Álvarez-Cuesta M and Le Cozannet G 2023 Demonstrating the value of beaches for adaptation to future coastal flood risk *Nat. Commun.* **14** 3474
[9] Liu G, Strong A E and Skirving W 2003 Remote sensing of sea surface temperatures during 2002 barrier reef coral bleaching *EOS* **84** 137–41
[10] Craighead F C and Gilbert V C 1962 The effects of Hurricane Donna on the vegetation of southern Florida *Q. J. Florida*

Acad. Sci. **25** 1–28 (available at: www.jstor.org/stable/24315186)
[11] Izaguirre C, Méndez F J, Menéndez M and Losada I J 2011 Global extreme wave height variability based on satellite data *Geophys. Res. Lett.* **38** 1–6
[12] Stopa J E and Cheung K F 2014 Periodicity and patterns of ocean wind and wave climate *J. Geophys. Res. Oceans* **119** 5563–84
[13] Reguero B G, Losada I J and Méndez F J 2015 A global wave power resource and its seasonal, interannual and long-term variability *Appl. Energy* **148** 366–80
[14] Semedo A, Sušelj K, Rutgersson A and Sterl A 2010 A global view on the wind sea and swell climate and variability from ERA-40 *J. Clim.* **24** 1461–79
[15] Echevarria E R, Hemer M A, Holbrook N J and Marshall A G 2020 Influence of the pacific-south american modes on the global spectral wind-wave climate *J. Geophys. Res. Oceans* **125** e2020JC016354
[16] Patra A, Min S K and Seong M G 2020 Climate variability impacts on global extreme wave heights: seasonal assessment using satellite data and ERA5 reanalysis *J. Geophys. Res. Oceans* **125** e2020JC016754
[17] Kumar P, Kaur S, Weller E and Min S K 2019 Influence of natural climate variability on the extreme ocean surface wave heights over the indian ocean *J. Geophys. Res. Oceans* **124** 6176–99
[18] Shimura T, Mori N and Mase H 2013 Ocean waves and teleconnection patterns in the Northern Hemisphere *J. Clim.* **26** 8654–70
[19] Odériz I, Silva R, Mortlock T R and Mori N 2020 ENSO impacts on global wave climate and potential coastal hazards *J. Geophys. Res. Oceans* **125** e2020JC016464
[20] Marshall A G, Hemer M A, Hendon H H and McInnes K L 2018 Southern annular mode impacts on global ocean surface waves *Ocean Model.* **129** 58–74
[21] Holbrook N J *et al* 2020 ENSO-driven ocean extremes and their ecosystem impacts *El Niño Southern Oscillation in a Changing Climate* ed M J McPhaden, A Santoso and W Cai pp 409–28
[22] Stone L, Huppert A, Rajagopalan B, Bhasin H and Loya Y 1999 Mass coral reef bleaching: a recent outcome of increased El Nino activity? *Ecol. Lett.* **2** 325–30
[23] Schoof J T and Pryor S C 2014 Assessing the fidelity of AOGCM-simulated relationships between large-scale modes of climate variability and wind speeds *J. Geophys. Res.* **119** 9719–34
[24] Wahl T and Plant N G 2015 Changes in erosion and flooding risk due to long-term and cyclic oceanographic trends *Geophys. Res. Lett.* **42** 2943–50
[25] Natural Earth 2023 *Natural Earth* (available at: www.naturalearthdata.com/downloads/)
[26] UNEP-WCMC WCWT 2021 Global Distribution of Warm-water Coral Reefs, Compiled from Multiple Sources Including the Millennium Coral Reef Mapping Project. Version 4.1. Includes Contributions from IMaRS-USF and IRD (2005), IMaRS-USF (2005) and Spalding *et al.* (2001) (UN Environment World Conservation Monitoring Centre)
[27] Bunting P, Rosenqvist A, Lucas R M, Rebelo L M, Hilarides L and Thomas N 2018 The global mangrove watch—A new 2010 global baseline of mangrove extent *Remote Sens.* **10** 1669
[28] Hersbach H, Bell B, Berrisford P, Hirahara S, Horányi A and Muñoz-Sabater J 2020 The ERA5 global reanalysis *Q. J. R. Meteorol. Soc.* **146** 1999–2049
[29] Odériz I, Silva R, Mortlock T R, Mori N, Shimura T and Webb A 2021 Natural variability and warming signals in global ocean wave climates *Geophys. Res. Lett.* **48** e2021GL093622
[30] Coles S 2001 *An Introduction to Statistical Modeling of Extreme Values* (Springer)
[31] Kumar P, Kaur S, Weller E and Young I R 2022 Influence of natural climate variability on extreme wave power over Indo-Pacific Ocean assessed using ERA5 *Clim. Dyn.* **58** 1613–33
[32] Timmermann A *et al* 2018 El Niño–southern oscillation complexity *Nature* **559** 535–45
[33] Chen S, Chen W, Yu B, Wu R, Graf H F and Chen L 2023 Enhanced impact of the Aleutian Low on increasing the Central Pacific ENSO in recent decades *npj Clim. Atmos. Sci.* **6** 29
[34] Barber R T, Hilting A K and Hayes M L 2001 The changing health of coral reefs *Hum. Ecol. Risk Assess.* **7** 1255–70
[35] Tuckett C A and Wernberg T 2018 High latitude corals tolerate severe cold spell *Front. Mar. Sci.* **5** 14
[36] Rimbu N, Lohmann G, Felis T and Pätzold J 2001 Arctic oscillation signature in a Red Sea coral *Geophys. Res. Lett.* **28** 2959–62
[37] Yadav S, Alcoverro T and Arthur R 2018 Coral reefs respond to repeated ENSO events with increasing resistance but reduced recovery capacities in the Lakshadweep archipelago *Coral Reefs* **37** 1245–57
[38] Manzello D P, Enochs I C, Bruckner A, Renaud P G, Kolodziej G and Budd D A 2014 Galápagos coral reef persistence after ENSO warming across an acidification gradient *Geophys. Res. Lett.* **41** 9001–8
[39] Hitt N T, Sinclair D J, Neil H L, Fallon S J, Komugabe-Dixson A, Fernandez D, Sutton P J and Hellstrom J C 2022 Natural cycles in south Pacific gyre strength and the southern annular mode *Sci. Rep.* **12** 18090
[40] Camargo S J, Robertson A W, Gaffney S J, Smyth P and Ghil M 2007 Cluster analysis of typhoon tracks. Part I General Properties *J. Clim.* **20** 3635–53
[41] Camargo S J, Robertson A W, Barnston A G and Ghil M 2008 Clustering of eastern North Pacific tropical cyclone tracks: ENSO and MJO effects *Geochem. Geophys. Geosyst.* **9** Q06V05
[42] Kuleshov Y, Qi L, Fawcett R and Jones D 2008 On tropical cyclone activity in the Southern Hemisphere: trends and the ENSO connection *Geophys. Res. Lett.* **35** L16805
[43] Enloe J, O'brien J J and Smith S R 2004 ENSO impacts on peak wind gusts in the united states *J. Clim.* **17** 1728–37
[44] Knapp P A and Hadley K S 2012 A 300-year history of Pacific Northwest windstorms inferred from tree rings *Glob. Planet. Change* **92–93** 257–66
[45] Angus M and Leckebusch G C 2020 On the dependency of Atlantic Hurricane and european windstorm hazards *Geophys. Res. Lett.* **47** e2020GL090446
[46] Brönnimann S 2007 Impact of El Niño-Southern Oscillation on European climate *Rev. Geophys.* **45** RG3003
[47] Screen J A, Bracegirdle T J and Simmonds I 2018 Polar climate change as manifest in atmospheric circulation *Curr. Clim. Change Rep.* **4** 383–95
[48] Deser C, Phillips A, Bourdette V and Teng H 2012 Uncertainty in climate change projections: the role of internal variability *Clim. Dyn.* **38** 527–46
[49] O'Reilly C H, Befort D J, Weisheimer A, Woollings T, Ballinger A and Hegerl G 2021 Projections of northern hemisphere extratropical climate underestimate internal variability and associated uncertainty *Commun. Earth Environ.* **2** 194
[50] Godwyn-Paulson P, Jonathan M P, Hernandez F R, Muthusankar G and Lakshumanan C 2020 Coastline variability of several Latin American cities alongside Pacific Ocean due to the unusual "Sea Swell" events of 2015 *Environ. Monit. Assess.* **192** 522
[51] Wang G, Cai W, Santoso A, Wu L, Fyfe J C and Yeh S-W 2022 Future Southern Ocean warming linked to projected ENSO variability *Nat. Clim. Change* **12** 649–54
[52] Cai W, Santoso A, Wang G, Yeh S-W, An S-I and Cobb K M 2015 ENSO and greenhouse warming *Nat. Clim. Change* **5** 849–59
[53] Santoso A, McGregor S, Jin F-F, Cai W, England M H, An S-I, McPhaden M J and Guilyardi E 2013 Late-twentieth-century emergence of the El Niño

propagation asymmetry and future projections *Nature* **504** 126–30
[54] Wang G and Cai W 2013 Climate-change impact on the 20th-century relationship between the Southern Annular Mode and global mean temperature *Sci. Rep.* **3** 2039
[55] Gan B, Wu L, Jia F, Li S, Cai W and Nakamura H 2017 On the response of the aleutian low to greenhouse warming *J. Clim.* **30** 3907–25
[56] Mentaschi L, Vousdoukas M I, Voukouvalas E, Dosio A and Feyen L 2017 Global changes of extreme coastal wave energy fluxes triggered by intensified teleconnection patterns *Geophys. Res. Lett.* **44** 2416–26
[57] Lee J-Y*et al* 2021 Future global climate: scenario-based projections and near-term information *Climate Change 2021: The Physical Science Basis. Contribution of Working Group I to the Sixth Assessment Report of the Intergovernmental Panel on Climate Change* ed V Masson-Delmotte *et al* (Cambridge University Press) pp 553–672
[58] Van der Stocken T and Menemenlis D 2017 Modelling mangrove propagule dispersal trajectories using high-resolution estimates of ocean surface winds and currents *Biotropica* **49** 472–81
[59] Van Der Stocken T *et al* 2013 *The role of wind in hydrochorous mangrove propagule dispersal* **10** 3635–47
[60] Kauffman J B and Cole T G 2010 Micronesian mangrove forest structure and tree responses to a severe typhoon *Wetlands* **30** 1077–84
[61] Peereman J, Hogan J A and Lin T C 2022 Disturbance frequency, intensity and forest structure modulate cyclone-induced changes in mangrove forest canopy cover *Glob. Ecol. Biogeogr.* **31** 37–50
[62] Wethey D S, Woodin S A, Hilbish T J, Jones S J, Lima F P and Brannock P M 2011 Response of intertidal populations to climate: effects of extreme events versus long term change *J. Exp. Mar. Bio. Ecol.* **400** 132–44
[63] Maza M, Lara J L and Losada I J 2022 A paradigm shift in the quantification of wave energy attenuation due to saltmarshes based on their standing biomass *Sci. Rep.* **12** 13883
[64] Odériz I, Losada I J, Silva R and Nobuhito M 2024 *Data for 'Global Assessment of Interannual Hazard Variability in Coastal Urban Areas and Ecosystems'* (Zenodo) (https://doi.org/10.5281/zenodo.11004723)